The Magnetic Self-Aligning Hermaphroditic Connector

A Scalable Approach for Modular Microrobots

Zoltán Nagy, Jake J. Abbott, and Bradley J. Nelson

***Abstract*— Modular microrobots will enable exploration and manipulation in tiny and difficult to access spaces. Modularity allows reconfiguration for adaptation to unstructured environments. In addition, individual modules can be designed for simple specific functions, thereby reducing fabrication complexity and easing downscaling. For modular microrobots, a robust connection mechanism is indispensable. In this paper, we introduce a magnetic self-aligning hermaphroditic connector. Self-alignment is achieved by a specific magnetic design that creates an attractive force, as well as a torque that aligns the mating faces into a known configuration. Each mating face is identical, and this hermaphroditic design, combined with self-alignment, provides a priori knowledge that once a mechanical connection is established, the intramodular communication system is also functional. Experiments with upscaled models demonstrate robust self-alignment and the desirable characteristics of the communication system. The use of magnets for the mechanical connection is the key for the scalability of the connector, as geometrical downscaling is favorable for magnet-magnet interaction and no moving parts are required. The analysis presented here will enable an optimal design of microscaled connectors.**

***Index Terms*— Self-alignement, reconfiguration, connection**

Fig. 1. Concept drawing of a modular microrobot. Relatively simple modules can be combined to form complex systems. The connection mechanism must allow for attraction and alignment of the modules to reduce control requirements and thus ensure robust self-assembly.

I. Introduction

Modular robots are robots that are composed of several units (the modules) of the same or of different kind. Using on-board actuators, these modules can be moved such that the robot can reconfigure into different shapes, thus allowing itself to adapt to different and unstructured environments. Since the late 1980s different research groups have presented their designs, placing emphasis on distinct aspects of the modularity, such as control, communication, locomotion, kinematics, etc. [1]–[9] (see [7], [10] for recent reviews).

Little work has been done on modular microrobots (MMR) [11]–[14]. The limiting factor being, among others, that the employed actuators (e.g. motors) and mechanical connection mechanisms (physical latching) cannot be scaled down easily to the microscale. MMR are of interest because they allow the same versatility as macroscaled modular robots, only at the microscale. Thus, in the future it will be possible to explore and perform manipulations in tiny regions that are difficult to access. In addition, it was stated in [15] that MMR will allow the physical implementation of the theoretical concept of stochastically reconfigurable microrobots.

In order to allow assembly and reconfiguration of MMR, a robust, reversible, and passive mechanical connection is indispensable. In addition, due to size limitations, only few sensors (if any) can be implemented in MMR. Consequently, proprioceptive sensory information will likely be reduced. Thus, the control required for connection (e.g., the alignment of the mating faces of two connectors) should be as simple as possible. The connection mechanism of an MMR should be compatible with microfabrication and/or microassembly processes and contain as few moving parts as possible.

It was claimed in [13] that magnetic latching is much more plausible than physical latching as size decreases to the micro- and nanoscale. In fact, it has been shown that geometrical downscaling is favorable for magnet-magnet interaction, in that the force per volume between two magnets is increased by the geometrical scaling factor, while the torque per volume remains constant [16].

In this paper, we present the concept for a MAgnetic Self-aligning Hermaphroditic (MASH) connector. Self-alignment is achieved by placing a magnetic dipole on the mating face and orienting it such that the connection takes place in the direction perpendicular to magnetization. As a consequence, the positions of the connectors relative to each other are known. This is exploited for the design of the intramodular communication system. The resulting hermaphroditic design offers robustness and reduced fabrication complexity.

Various connection mechanisms using magnets have been proposed in the past, however, none of them fulfills our

This work was supported by the European Commission in the framework of the 6FP NEST Adventure Project ARES.

The authors are with the Institute of Robotics and Intelligent Systems, ETH Zurich, Switzerland {nagyz,jabbott,bnelson}@ethz.ch

1-4244-1264-1/07/$25.00 ©2007 IEEE

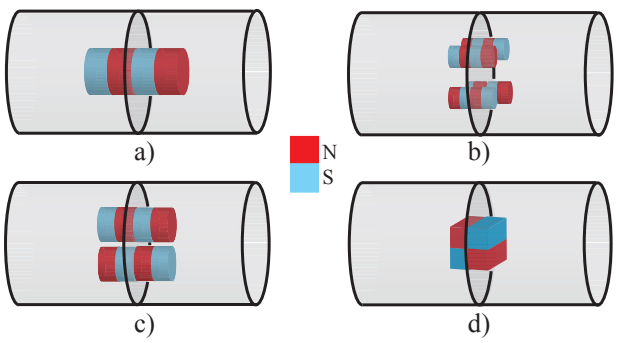

Fig. 2. a) With only one pole on each connector, undesired rotation along the magnetization axis is possible. b) With multiple poles on the connection face, misalignments are still possible. c) Exactly two poles on a face ensure a unique configuration and self-alignment once the connectors are close. d) A single magnet oriented perpendicular to the connection axis shows similar characteristics.

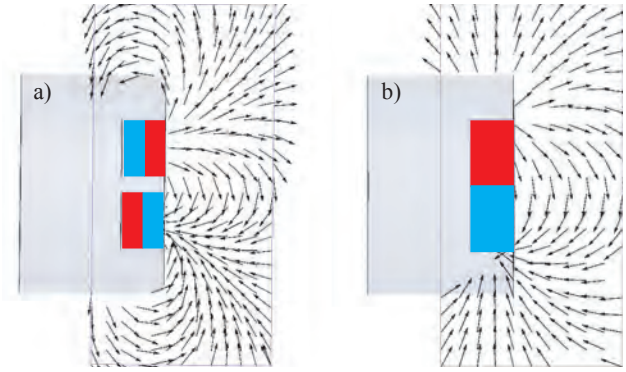

Fig. 3. The field line plots indicate that the one-magnet configuration b) is more likely to provide robust self-assembly. a) and b) correspond to Fig. 2c) and d) respectively.

requirements. The self-aligning mechanism described in [4] requires that the mating faces are brought together prealigned at a certain distance in order to avoid misalignments. In [2] and [13] electromagnets are used to alter the magnetic fields to allow disconnection. Yet, magnetic induction is very poor when downscaling and thus less effective at the microscale [16].

This paper is organized as follows. Section II introduces the concept of the connector and discusses design aspects. The magnetic interaction is analyzed in Section III and the experimental results are presented in Section IV. Section V concludes the paper and gives outlook to future work.

II. The MASH Concept

A. Magnetic Self-Alignment

In this section, we explore the magnetic design of the connector. The design must allow for robust attraction and self-alignment of the modules to reduce control requirements. In addition, a hermaphroditic connector face must also allow the largest number of possible configurations to increase the likelihood of successful self-assembly.

The design of the MASH connector is based on the well-known magnetic interaction mechanism: opposite poles will attract and like poles will repel. Thus, a north pole on one connector will always attract a south pole on another connector, providing a robust attraction mechanism.

However, it is not enough to provide attraction, as rotation around the magnetization axis may still be possible (see Fig. 2a)). Also, the hermaphroditic requirement must be fulfilled. For the latter, both south and north poles have to be present on the connector face. This can be done by multiple configurations, and one example is shown in Fig. 2b). Still, these configurations are prone to unwanted but stable misaligned states.

Now consider configurations where exactly two poles are present on the face. Possible realizations are with two distinct magnets (Fig. 2c)) or with one magnet (Fig. 2d)), oriented such that the connection takes place along an axis perpendicular to the magnetization of the magnet. In both cases, any misalignment (or displacement) of the two connecting faces relative to each other gives rise to a restoring torque (force) that realigns (reconnects) the modules. Hence, a robust connection is ensured for disturbing torques and forces lower than some critical values. This is the configuration of the MASH connector.

It is not obvious which of the two possible configurations optimally fulfills the requirements for both attraction and self-alignment. The field line plots indicate that the one magnet configuration (Fig. 3b)) is more likely to provide robust self-assembly, as the magnet on the other mating face will tend to align itself along the field lines. In the configuration shown in Fig. 3a), one-magnet may dominate the interaction and lead to a misaligned connection. Consequently, in this paper we will concentrate on the one-magnet configuration. A detailed analysis of both configurations will be the subject of future work.

B. Hermaphroditic Communication Connection

Due to the self-alignment of the connectors, a hermaphroditic design can be obtained for the electrical contacts of the mating faces as shown in Fig. 4. Consider two identical connectors $\mathcal{C}_1$ and $\mathcal{C}_2$. The contact point A of $\mathcal{C}_1$ connects to the contact point A' of $\mathcal{C}_2$. Now, for a hermaphroditic design, A has to be present on $\mathcal{C}_2$ at the same position with respect to the magnet. Likewise, A' has a well-defined position on $\mathcal{C}_1$. This procedure of designing the location of the contact points can be carried out systematically as shown in Fig. 4. In a physical implementation, all points carrying the same signal, e.g. A and A', are shorted together within the module. Consequently, if one of the two $A-A'$ connections on each mating face fails, the signal is still transmitted.

The shape of the mating faces is independent on this procedure and hence arbitrary connector shapes are possible. In addition, the number of the contact points is only limited by their size and the size of the mating face of the connector. Finally, note, that the MASH concept is not limited to electrical signals. Wireless infra-red (IR) communication is also possible without violating the hermaphroditic nature of the connector. For example, A could be an IR emitter and A' an IR receiver.

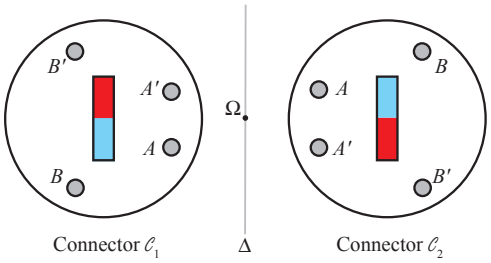

Fig. 4. When two identical connectors are arranged as shown, a hermaphroditic configuration is obtained by requiring that mating contact points $A - A'$ are images of each other through the reflection with respect to the axis Δ and same contact points on different connectors are images of each other through the point reflection with center Ω. In the figure, the locations of A and B are arbitrary, but they induce the locations of A' and B'.

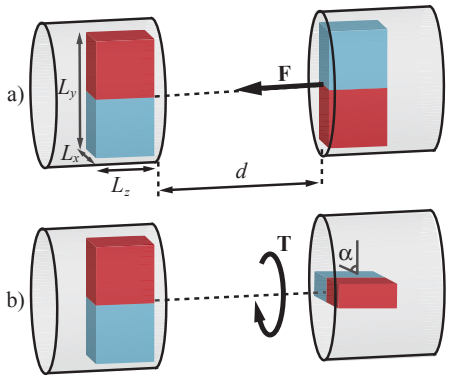

Fig. 5. The studied configurations for the FE analysis of the force and torque between two magnets

III. Analysis of Magnetic Interaction

The magnetic force $\mathbf{F}$ and torque $\mathbf{T}$ acting on a magnet $\mathcal{M}_1$ with a magnetic dipole moment $\mathbf{\Gamma}$ (units in Am^2) in an external field $\mathbf{H}$ (units in $\mathrm{A/m}$) is given by

$$\mathbf{F} = \mu_0(\mathbf{\Gamma}\cdot\nabla)\mathbf{H} \quad (1)$$

$$\mathbf{T} = \mu_0\mathbf{\Gamma}\times\mathbf{H} \quad (2)$$

where $\mu_0 = 4\pi\times10^{-7}\,\mathrm{Tm/A}$ is the permeability of free space. Note, the magnetic dipole moment is related to the magnetization of the material $\mathbf{M}$ (units in $\mathrm{A/m}$) by the volume V of $\mathcal{M}_1$: $\mathbf{\Gamma} = V\mathbf{M}$. All vectors are expressed in the same frame. Now, consider that the source of $\mathbf{H}$ is another magnet $\mathcal{M}_2$. The field can be approximated using the point dipole model [17], as

$$\mathbf{H}(\mathbf{P}) = \frac{1}{4\pi|\mathbf{P}|^3}\left(\frac{3(\mathbf{\Gamma}\cdot\mathbf{P})\mathbf{P}}{|\mathbf{P}|^2} - \mathbf{\Gamma}\right) \quad (3)$$

where $\mathbf{\Gamma}$ is the magnetic moment of $\mathcal{M}_2$, $\mathbf{P}$ is the vector from the point dipole to the position of interest and $\mathbf{\Gamma}$, $\mathbf{P}$, and $\mathbf{H}$ are expressed with respect to the same coordinate frame.

Other models are available, that attempt to capture the physical dimensions of the magnet (for example the charge model or the current model [18]). However, the drawback of all three models is that they are only valid for relatively large values of $|\mathbf{P}|$. Consequently, (1) and (2) can be used to analyze magnet-magnet interaction at relatively large separations but they cannot accurately model the interaction during the whole connection phase.

The strength of the connection is dependent on (among other things) the size, the aspect ratio, and the orientation of the magnets, as well as on the distance between the magnets. We measured the force between two NdFeB rare-earth magnets from Supermagnete.ch (Q-19-13-06-LN) by gluing one magnet to an aluminum substrate and placing it onto a precision scale (Acculab VI1-MG). The other magnet was mounted to a micropositioning stage from Sutter Instruments (MP-285). The orientation of the magnets is as shown in Fig. 5a), and the distance d between the magnets is varied. The dimensions of the magnets are $L_x = 6.4\mathrm{mm}$, $L_y = 19.1\mathrm{mm}$, $L_z = 12.7\mathrm{mm}$ and their remanence is $1.2\mathrm{T}$. The further investigation of the magnetic interaction is done by finite element (FE) simulations using the commercial FE software Maxwell [19]. We validated the FE results by analyzing the same configuration as our experiment. We found good agreement between the simulations and the experimental results (see Fig. 6, $\gamma = 1$).

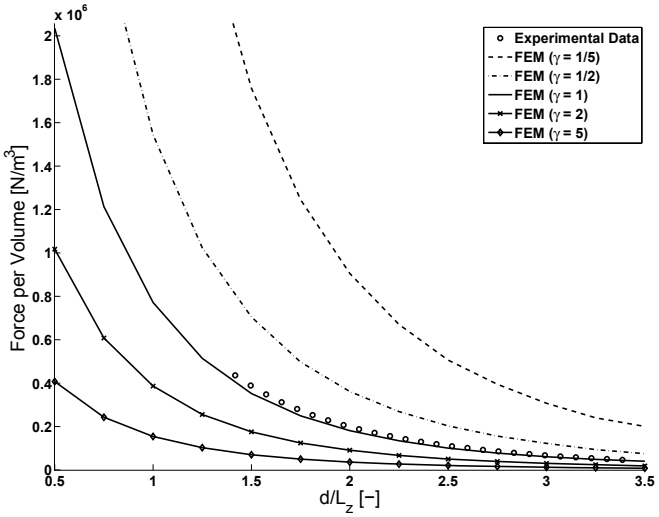

Fig. 6. Good agreement is found between the experimental data (circles) and the FE simulation ($\gamma = 1$). It can be observed that the force per volume increases for $\gamma < 1$ as predicted [16]. Note that the measured forces are the upper limit of our experimental setup.

Next, we used the FE model to verify the scaling effects predicted in [16]—i.e., that the force per volume is multiplied by the inverse of the geometrical scaling factor $1/\gamma$. Thus, we considered the force between two magnets with sidelengths $(\gamma L_x, \gamma L_y, \gamma L_z)$ at the distance $d = \gamma L_z$, with $\gamma \in \{\frac{1}{5}\ldots5\}$. As shown in Fig. 6, the predictions are confirmed.

The same analysis has also been performed for the restoring torque at the configuration shown in Fig. 5b) with $\alpha = 90°$: the torque as a function of d/L_z and the effects of geometrical scaling by γ. The results are shown in Fig. 7. As predicted, the torque per volume remains constant for

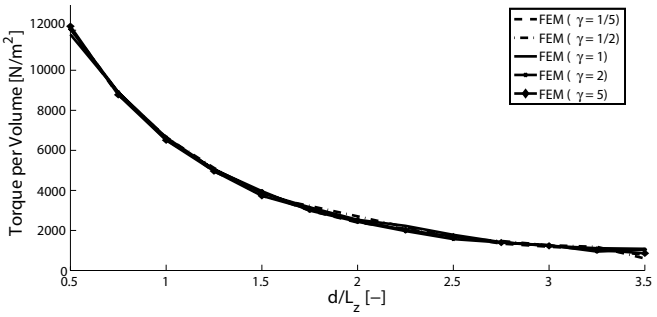

Fig. 7. FE analysis showing the torque per volume ratio, which remains constant for different γ.

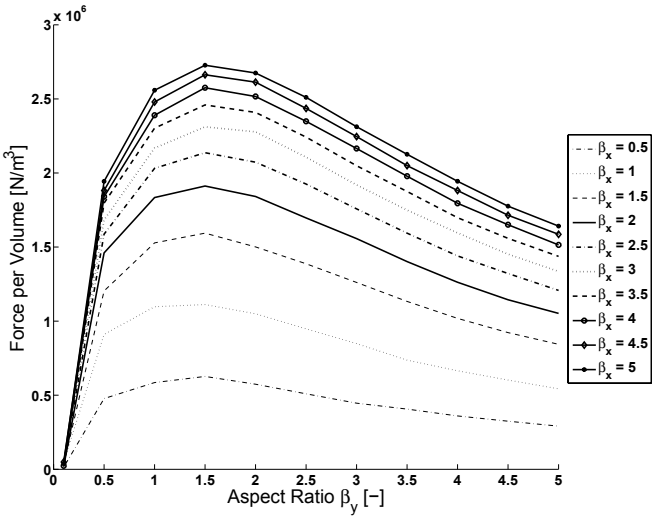

Fig. 8. FE analysis showing the influence of the aspect ratios $\beta_x = \frac{L_x}{L_z}$ and $\beta_y = \frac{L_y}{L_z}$ on the force between the magnets ($d = L_z$). We observe that the force per volume increases with β_x and shows a maximum for $1 < \beta_y < 2$.

different γ.

Finally, we investigated the influence of the aspect ratios $\beta_x = \frac{L_x}{L_z}$ and $\beta_y = \frac{L_y}{L_z}$ on the force (with $d = L_z$) and the restoring torque (with $d = L_z$ and $\alpha = 90°$) between the magnets. The results are shown in Figs. 8 and 9. We observe that both the force and the torque per volume increase with β_x and show a maximum for some $\beta_y = \beta_{y,\max}$. For the force, we find $1 < \beta_{y,\max} < 2$ for the considered β_x. For the torque, however, $\beta_{y,\max}$ increases with increasing β_x.

IV. Experimental Results

A. Prototype Fabrication

Upscaled models of the MASH connector were fabricated from PMMA with conventional fabrication techniques. The shape of the connectors is cylindrical with a diameter of 50 mm and a height of 17 mm. The magnets were glued into the machined openings using a two-component glue. Eight holes are designed for communication connections, thus four distinct datalines can be used due to the symmetry conditions imposed by the hermaphroditic design (see Section II-B).

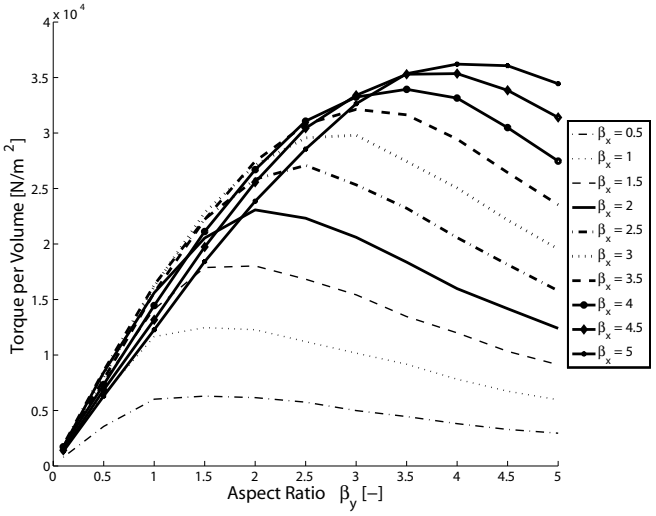

Fig. 9. FE analysis showing thenfluence of the aspect ratios $\beta_x = \frac{L_x}{L_z}$ and $\beta_y = \frac{L_y}{L_z}$ on the torque between the magnets ($d = L_z$, $\alpha = 90°$). We observe that the torque per volume increases with β_x and that the position of the maximum increases also with β_x.

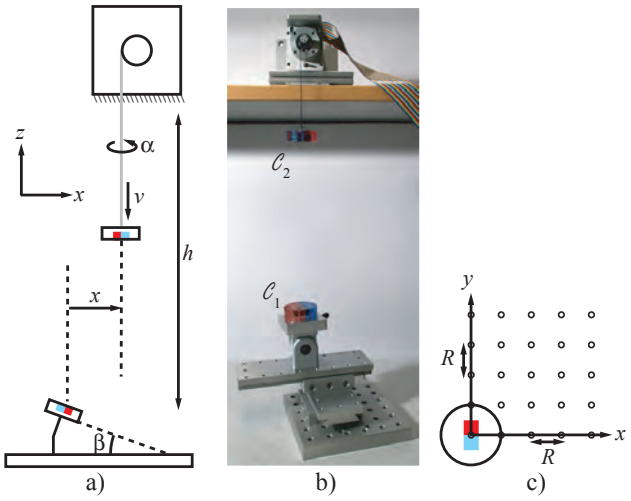

Fig. 10. Experimental Setup: a) sketch, b) actual setup and c) the explored parameter space. See text for explanations.

Two experiments were performed to demonstrate the concept of the MASH connector. First we show the alignment performance, then the communication system.

B. Alignment Performance

The experimental setup is shown in Fig. 10. One connector ($\mathcal{C}_1$) is mounted on an 3DOF stage (lateral motion in x and y and rotation by β). The other connector ($\mathcal{C}_2$) is attached to a DC motor by means of an elastic string. Also, by rotating the linear stage about the z axis, the angle α can be set (the same as in Fig. 5b)). In the experiments, $\mathcal{C}_2$ is lowered at a slow constant speed of $v \approx 2.5\,\mathrm{mm/s}$ from a height $h = 35\,\mathrm{cm}$, thus we consider quasi-static conditions. We explore the parameter space $x, y \in \{0, R, 2R, 3R, 4R\}$, with $R = 25\,\mathrm{mm}$ being the radius of the connectors and x

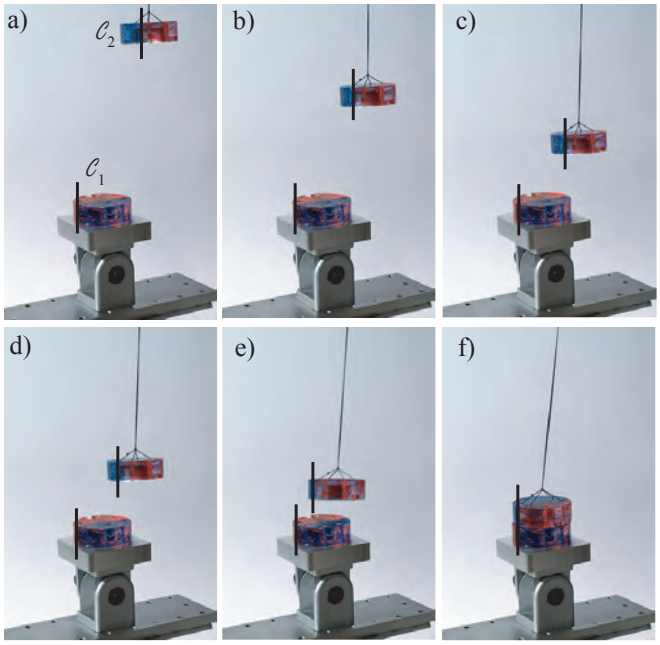

Fig. 11. Typical Experiment. First, long range interaction may lead to rotation of $\mathcal{C}_2$ a),b). In the medium range c),d) the magnetic interaction starts to dominate over gravity and the elasticity of the string leading to lateral displacement of $\mathcal{C}_2$. Finally, self-alignment is achieved in the short range e),f). In the figure, the black line indicates the midline between the south and the north pole.

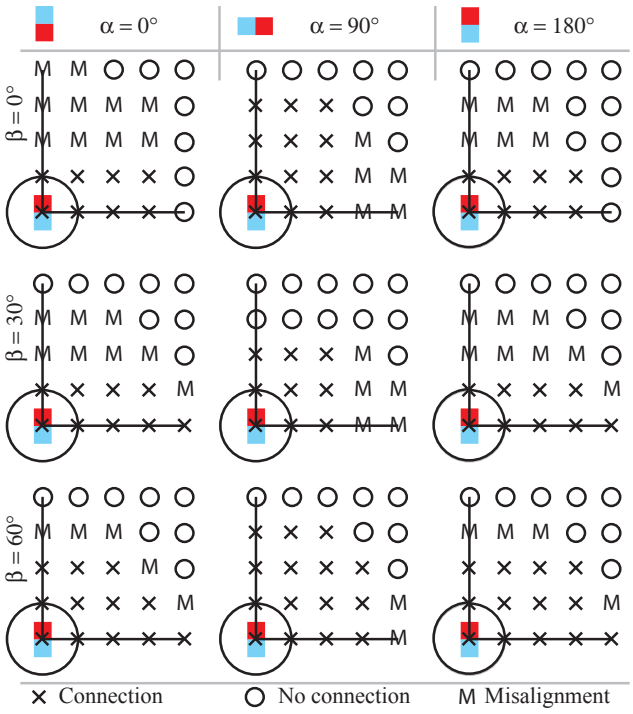

Fig. 12. Experimental Results. Note that with this setup, connections from distances as large as $4R$ are achievable, and connections from distances of up to R are always achieved.

and y the distance between the center of the connectors. Also, we consider the angles $\alpha \in \{0°, 90°, 180°\}$, and $\beta \in \{0°, 30°, 60°\}$, and determine whether a connection is achieved or not. A typical experiment is shown in Fig. 11 ($x = R, y = R, \alpha = 90°, \beta = 0°$), and the complete results are shown in Fig. 12. We can distinguish three phases of interaction: 1) Long range interaction. Depending on x, y, and α, this may lead to rotation of $\mathcal{C}_2$ (e.g. for $(x, y, \alpha) = (0, 2R, 90°)$). 2) In the medium range, the magnetic interaction starts to dominate over gravity and the elasticity of the string, leading to lateral displacement of $\mathcal{C}_2$. 3) At the short range, all four poles interact and $\mathcal{C}_2$ aligns with $\mathcal{C}_1$. If the magnetic interaction in the medium range is too weak, misalignment or non-connection can occur (as shown in Fig. 12). Note that with this setup, aligned connections from distances as large as $4R$ are achievable.

We observe that in each of the configurations a connection is achieved if the connectors are sufficiently close to each other in x and y. Thus, robust self-alignment is possible. In addition, the best results are not achieved for $\alpha = 0°, \beta = 0°$, hence perfect angular alignment does not necessarily leads to the most efficient connection.

Of course, taking into account that for example the geometry of the connectors, the elasticity of the string, and the speed of the DC motor have not been considered, these results are only of qualitative nature. However, we can conclude that there exists a region in the parameter space in which the connectors have to be brought together in order to self align and to form a robust connection. This region has to be determined for each specific connector design.

C. Communication System

To demonstrate the advantage of the hermaphroditic design, we fabricated three different protomodules and attached two connectors to each of them. The three modules were given different functions: a power module providing a $V_{cc} = 4.5\,\mathrm{V}$ and the GND signal, a switching module allowing to set the datalines A and B to high or low, and the logic module that determines the battery state and evaluates the inputs of the switching module by an XOR and an AND gate (see Fig. 13a)-c) and Fig. 14). The electrical signals between two mating connectors were transmitted by screws, for the ease of fabrication.

Fig. 13d) shows the three modules connected as Switch-Power-Logic and Fig. 13e) as Power-Logic-Switch. Note the different shining LEDs on the Logic module that determine that in d) both switches in the Switch module are set to the same state (orange LED), while in e) the switches are in opposite state (red LED). The green LED indicates that power is available.

At first consideration, using multiple datalines for communication might seem overdesigned, as for example, serial communication could be used instead. However, consider that due to the size constraints, modular microrobots (MMR) may be heterogeneous and logic signals might be the most viable form of communication. In addition, the MASH connector offers communication robustness due to its redundant design, because data sent through dataline A, for example,

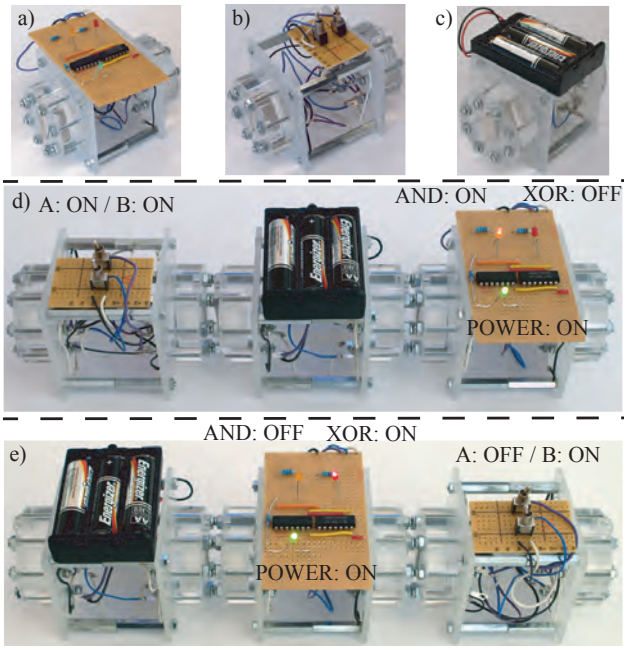

Fig. 13. Three modules with different functions have been fabricated to demonstrate the hermaphroditic design: a) a logic module, b) a switch module and c) a power module. In d) and e) the modules are differently arranged and the switch module has different settings, resulting in different outputs of the logic module.

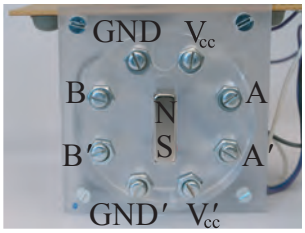

Fig. 14. The MASH connector mounted on a module, with wiring diagram.

is additionally sent through dataline A'. Finally, in each module, the equivalent contact points on one connector (e.g. A and A') are shorted, thus only one of them is required to propagate the signal through the module.

V. Conclusions and Future Work

We have demonstrated a scalable concept of a connector that allows robust mechanical connection between different modules of a modular microrobot. Our experiments show that self-alignment can be achieved even for relatively large lateral displacements between two connectors. In addition, the hermaphroditic design allows the implementation of a simple but robust communication bus. The combination of the MASH connector with scalable and low power actuators such as those in [20] offer the prospect of true modular microrobots.

Further research is required in development of a fabrication process to produce a MEMS based connector (μMASH), design of a MEMS-compatible disconnection mechanism, and design and fabrication of different micromodules. The analysis of magnetic interaction presented here will be used in the optimal design of μMASH. The disconnection mechanism can be analogous to [4], which uses a scalable actuator (based on shape memory alloy) and nonlinear springs that could be replaced by a deflecting micromembrane.

Finally, note that the MASH concept is not only valid for the micro- and nanoscale or for modular robots. In fact, it can be used in any situation where hardly accessible components have to be joined, or where manipulation capabilities are reduced (e.g. in space).

References

[1] T. Fukuda and S. Nakagawa, "Approach to the dynamically reconfigurable robotic system," *J. Intelligent and Robotic Systems*, pp. 55–72, 1988.

[2] S. Murata, H. Kurokawa, and S. Kokaji, "Self-assembling machine," in *IEEE Int. Conf. Robotics and Automation*, 1994, pp. 441–448.

[3] M. Yim, Z. Ying, K. Roufas, D. Duff, and C. Eldershaw, "Connecting and disconnecting for chain self-reconfiguration with polybot," *IEEE/ASME Trans. Mechatronics*, vol. 7, no. 4, pp. 442–451, 2002.

[4] S. Murata, E. Yoshida, A. Kamimura, H. Kurokawa, K. Tomita, and S. Kokaji, "M-tran: self-reconfigurable modular robotic system," *IEEE/ASME Trans. Mechatronics*, vol. 7, pp. 431–441, 2002.

[5] W.-M. Shen, B. Salemi, and P. Will, "Hormone-inspired adaptive communication and distributed control for CONRO self-reconfigurable robots," *IEEE Trans. Robotics and Automation*, vol. 18, no. 5, pp. 700–712, 2002.

[6] A. Brunete, M. Hernando, and E. Gambao, "Modular multiconfigurable architecture for low diameter pipe inspection microrobots," in *IEEE Int. Conf. Robotics and Automation*, 2005, pp. 490–495.

[7] E. H. Ostergaard, K. Kassow, R. Beck, and H. H. Lund, "Design of the ATRON lattice-based self-reconfigurable robot," *Autonomous Robots*, vol. 21, no. 2, pp. 165–183, 2006.

[8] R. Moeckel, C. Jaquier, K. Drapel, E. Dittrich, A. Upegui, and A. J. Ijspeert, "Exploring adaptive locomotion with YaMoR, a novel autonomous modular robot with bluetooth interface," *Industrial Robot: An Int. Journal*, vol. 33, no. 4, pp. 285–290, 2006.

[9] J. W. Suh, S. B. Homans, and M. Yim, "Telecubes: mechanical design of a module for self-reconfigurable robotics," in *IEEE Int. Conf. Robotics and Automation*, 2002, pp. 4095–4101.

[10] M. Yim, S. Wei-Min, B. Salemi, D. Rus, M. Moll, H. Lipson, E. Klavins, and G. S. Chirikjian, "Modular self-reconfigurable robot systems [grand challenges of robotics]," *IEEE Robotics & Automation Magazine*, vol. 14, no. 1, pp. 43–52, 2007, 1070-9932.

[11] H. Ishihara, T. Fukuda, K. Kosuge, F. Arai, and K. Hamagishi, "Approach to distributed micro robotic system: Development of microline trace robot and autonomous micro robotic system," in *IEEE Int. Conf. Robotics and Automation*, 1995, pp. 375–380.

[12] E. Yoshida, S. Kokaji, S. K. Murata, and K. H. Tomita, "Miniaturized self-reconfigurable system using shape memory alloy," in *IEEE/RSJ Int. Conf. Intelligent Robots and Systems*, 1999, pp. 1579–1585.

[13] S. A. Patterson, K. A. J. Knowles, and B. E. Bishop, "Toward magnetically-coupled reconfigurable modular robots," in *IEEE Int. Conf. Robotics and Automation*, 2004, pp. 2900–2905.

[14] J. Campbell, P. Pillai, and S. C. Goldstein, "The robot is the tether: active, adaptive power routing modular robots with unary inter-robot connectors," in *IEEE/RSJ Int. Conf. Intelligent Robots and Systems*, 2005, pp. 4108–4115.

[15] P. J. White, K. Kopanski, and H. Lipson, "Stochastic self-reconfigurable cellular robotics," in *IEEE Int. Conf. Robotics and Automation*, 2004, pp. 2888–2893.

[16] O. Cugat, J. Delamare, and G. Reyne, "Magnetic micro-actuators and systems (MAGMAS)," *IEEE Trans. Magnetics*, vol. 39, no. 5, pp. 3607–3612, 2003.

[17] B. D. Cullity, *Introduction to Magnetic Materials*. Reading, MA: Addison-Wesley, 1972.

[18] E. P. Furlani, *Permanent Magnet and Electromechanical Devices*. San Diego, CA: Academic Press, 2001.

[19] (2007) Ansoft Inc. [Online]. Available: http://www.ansoft.com

[20] N. Ng Pak, R. J. Webster III., A. Menciassi, and P. Dario, "Electrolytic silicone bourdon tube microactuator for reconfigurable surgical robots," in *IEEE Int. Conf. Robotics and Automation*, 2007, pp. 3371–3376.